AGU100 ADVANCING EARTH AND SPACE SCIENCE

JGR

Journal of Geophysical Research: Oceans

RESEARCH ARTICLE
10.1029/2018JC014388

Key Points:
- This is the first analysis of the deterioration occurring from ice islands generated by Petermann Glacier calving events
- A power law model best represented size distributions, and meltwater fluxes were elevated in Petermann Fjord and near ice island groundings
- These analyses were conducted with the CI2D3 Database, which contains >17,000 entries of Petermann ice islands of interest

Correspondence to:
A. J. Crawford,
anna.crawford@carleton.ca

Citation:
Crawford, A. J., Mueller, D., Desjardins, L., & Myers, P. G. (2018). The aftermath of Petermann Glacier calving events (2008–2012): Ice island size distributions and meltwater dispersal. *Journal of Geophysical Research: Oceans*, *123*, 8812–8827. https://doi.org/10.1029/2018JC014388

Received 20 JUL 2018
Accepted 2 NOV 2018
Accepted article online 5 NOV 2018
Published online 5 DEC 2018

The Aftermath of Petermann Glacier Calving Events (2008–2012): Ice Island Size Distributions and Meltwater Dispersal

Anna J. Crawford[1], Derek Mueller[1], Luc Desjardins[1,2], and Paul G. Myers[3]

[1]Water and Ice Research Lab, Department of Geography and Environmental Studies, Carleton University, Ottawa, Ontario, Canada, [2]Canadian Ice Service, Environment and Climate Change Canada, Ottawa, Ontario, Canada, [3]Department of Earth and Atmospheric Sciences, University of Alberta, Edmonton, Alberta, Canada

Abstract Three large calving events occurred at Petermann Glacier in northwest Greenland between 2008 and 2012 that generated ice islands (large tabular icebergs) that ranged from ~30 to 300 km^2 in areal extent. Ice islands are known to deteriorate, via fracture and melt, during their drift through regional water bodies where they pose a potential risk to offshore resource extraction operations and disperse freshwater from the Greenland Ice Sheet. This study presents the first analysis of the deterioration occurring across the flux of ice islands that travel between Nares Strait and the North Atlantic after Petermann Glacier calving events. The evolution of Petermann ice island size distributions was evaluated, and the spatial dispersal of meltwater was quantified, through analyses that utilized the newly developed Canadian Ice Island Drift, Deterioration and Detection Database. Size-frequency distributions remained relatively consistent, both spatially and temporally, and were well fit by power law models with slopes of approximately −1.7. This suggested that fracture was an important process by which the Petermann ice islands deteriorated, regardless of elapsed time or distance from the glacier. Ice island meltwater fluxes into the Baffin Island and Labrador currents were not large enough to slow down the Atlantic Meridional Overturning Circulation by weakening deep-water convection in the Labrador Sea. However, augmented meltwater input was calculated within Petermann Fjord (2.0 mSv) and in the vicinity of grounding locations (0.4 mSv). Further research is necessary to better understand how this freshwater alters fjord circulation and influences the composition of local ocean waters.

Plain Language Summary Three large tabular icebergs ("ice islands") broke away from Petermann Glacier, northwest Greenland, between 2008 and 2012. We use the Canadian Ice Island Drift, Deterioration and Detection Database to investigate the ice island size distributions as well as how meltwater, generated through their drift and deterioration, is dispersed through water bodies such as Baffin Bay and the Labrador Sea. The size-frequency distributions were best fit by power law models, which suggests that fracture was an important process by which the Petermann ice islands deteriorated. While augmented meltwater input was calculated within Petermann Fjord and at grounding locations, ice island meltwater fluxes were not large enough to slow down the Atlantic Meridional Overturning Circulation. Our results contribute to the two dominant themes of ice island research: their role in the dispersal of freshwater from the major Arctic and Antarctic ice sheets and the risk that they pose to shipping and offshore resource extraction operations.

1. Introduction

Large tabular icebergs, or "ice islands," are generated by calving events at high-latitude ice shelves and floating ice tongues (Bigg et al., 2014; Nick et al., 2012). Examples include the 5,800-km^2 ice island that broke away from Larsen-C Ice Shelf in Antarctica in 2017 and three large ice islands that calved in relatively rapid succession between 2008 and 2012 from Petermann Glacier in northwest Greenland (Crawford, Crocker, et al., 2018; Münchow et al., 2014; National Aeronautics and Space Administration, 2017). While smaller than many of their Antarctic counterparts, these three ice islands (~30 to 300 km^2) were more extensive than typical Arctic ice islands (Figure 1; Crawford, Crocker, et al., 2018; Newell, 1993).

Research concerning ice islands and the many ice island fragments produced during their deterioration has predominantly been dedicated to two subjects: their potential as hazards to shipping and offshore industrial operations (Fuglem & Jordaan, 2017; Haas, 2012; McGonigal et al., 2011; Mueller et al., 2013; Peterson, 2011) and the dispersal of fresh meltwater as they deteriorate during drift (Gladstone et al., 2001; Merino et al., 2016;

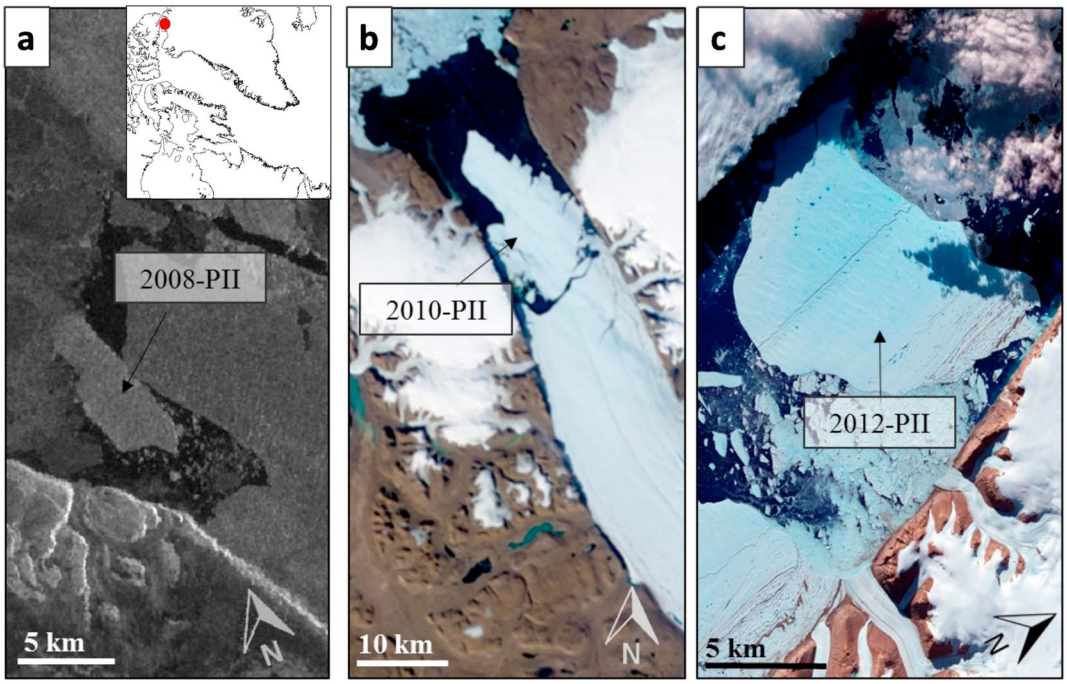

Figure 1. Ice islands produced by recent calving events at the Petermann Glacier. (a) July 2008, Envisat (© European Space Agency); (b) August 2010, MODIS Aqua (NASA, 2010); and (c) July 2012, ASTER Terra (NASA, 2012). The location of Petermann Glacier is denoted by the red circle in Figure 1a. MODIS = Moderate Resolution Imaging Spectroradiometer; NASA = National Aeronautics and Space Administration; ASTER = Advanced Spaceborne Thermal Emission and Reflection Radiometer; PII = Petermann ice island.

Silva et al., 2006; Smith, 2011). Arctic research has historically focused on the former, as ice islands fracture and generate numerous smaller ice islands, and icebergs, as well as bergy bits (100–300 m^2) and growlers (20 m^2), which represent hazards to regional industrial interests (Canadian Ice Service [CIS], 2005; Newell, 1993; Peterson, 2011; Peterson et al., 2009; Sackinger et al., 1985).

Antarctic research has concentrated on the distribution of meltwater inputs into the Southern Ocean resulting from the melt of ice islands, as well as the resulting biological, physical, and chemical consequences to the surrounding water column (Duprat et al., 2016; Helly et al., 2011; Raiswell et al., 2016; Smith et al., 2013). A series of studies beginning in 1980 used shipborne observations to assess the distribution patterns of Antarctic ice island fragments and to infer rates of deterioration through size and concentration data (Budd et al., 1980; Hamley & Budd, 1986; Jacka & Giles, 2007; Romanov et al., 2012). The most recent additions to this research by Tournadre et al. (2012, 2015, 2016) incorporated altimeter, scatterometer, and optical and synthetic aperture radar (SAR) remote sensing data sets (Fletcher et al., 2016; Long et al., 2002; Stuart & Long, 2011), which greatly increased the spatial coverage of the distribution analyses and also extended the size classes included within the data set.

Ice islands and icebergs are an important component of the freshwater flux from the Antarctic and Greenland ice sheets due to their potential to distribute meltwater over large regions (Enderlin et al., 2016, 2018; Luckman et al., 2010; Stern et al., 2015). More concerted research is now being undertaken on this topic in Arctic and sub-Arctic waters (Enderlin et al., 2016; Marson et al., 2018; Stern et al., 2015; Wagner & Eisenman, 2017). However, it is a challenge to monitor numerous ice islands over their entire life spans (Merino et al., 2016; Rackow et al., 2017; Stern et al., 2016). This has made it difficult to analyze deterioration and estimate the spatial and temporal dispersal of meltwater following specific ice island calving events.

This article touches upon both of these research themes by using the new Canadian Ice Island Drift, Deterioration and Detection (CI2D3) Database (Crawford, Crocker, et al., 2018) to investigate the downstream consequences of the 2008, 2010, and 2012 Petermann Glacier calving events. This study determines the fit of several statistical distributions to the size-frequency distribution of Petermann ice islands (PIIs) to evaluate which one provides the best representation of these ice island observations. Iceberg and ice islands in the

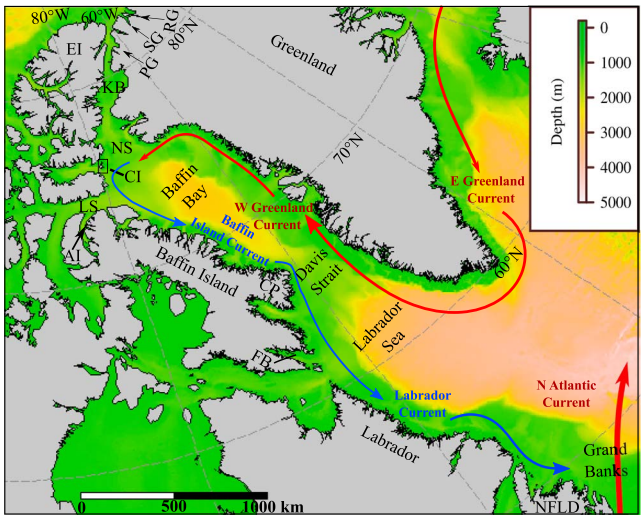

Figure 2. Bathymetry and ocean currents in the study area (National Geophysical Data Center, 2006). PG = Petermann Glacier; RG = Ryder Glacier; SG = Steensby Glacier; KB = Kane Basin; LS = Lancaster Sound; NFLD = Newfoundland; CP = Cumberland Peninsula; AI = Admiralty Inlet; CI = Coburg Island EI = Ellesmere Island; NS = Nares Strait; FB = Frobisher Bay. Warm and cold currents are denoted by the red and blue colors, respectively.

Arctic and Antarctic have previously been described to be well represented by log-normal or power law size-frequency distributions (Enderlin et al., 2016; Kirkham et al., 2017; Stern et al., 2016; Tournadre et al., 2015). The nature of these distributions reflect the processes (e.g., fracture, smaller-scale calving, and wave erosion) that contribute to iceberg or ice island deterioration (Kirkham et al., 2017), which then influences the number and size of ice hazards and meltwater production. The results of our analysis are discussed in this context.

This study also identifies where augmented, fresh meltwater flux magnitudes occur in eastern Canadian Arctic waterbodies after ice island calving events at Petermann Glacier. We quantify the spatial distribution of meltwater resulting from the drift and deterioration of the numerous ice islands that originated from the 2008, 2010, and 2012 Petermann Glacier calving events and discuss the potential consequences of this meltwater flux over varying spatial scales. The CI2D3 Database tracks the lineage of ice islands until they decrease to approximately 0.25 km^2 in surface area (Crawford, Desjardins, et al., 2018). It is this lineage information and thorough monitoring that made it possible to conduct these analyses for the individual PIIs observed in satellite-borne SAR imagery that was acquired between July 2008 and December 2013.

2. Study Area

Northwest Greenland contains a number of glaciers (i.e., Petermann, Ryder, and Steensby glaciers) that terminate in floating ice tongues and episodically calve large ice islands (Figure 2; Higgins, 1989). Petermann Glacier itself drains approximately 4% of the surface area of the Greenland Ice Sheet and has, historically, been observed to calve once every 5 to 10 years (Higgins, 1991; Münchow et al., 2014). Recent calving events occurred in 2001, 2008, 2010, 2011, 2012, 2013, and 2017 (Crawford, Crocker, et al., 2018; Desjardins et al., 2018).

Ice islands that calve from the northwest Greenland ice tongues fracture into numerous individual ice islands that follow a southward drift trajectory. Figure 2 illustrates the dominant currents and bathymetry that influence ice island drift routes through the study area. Ice islands become caught in the southward flowing Baffin Island Current after passing over a sill separating Kane Basin from Baffin Bay (Fissel, 1982; Tang et al., 2004). Ice islands typically follow the edge of the Baffin Island continental shelf next to a steep shelf break (Newell, 1993; Tang et al., 2004). They exit Baffin Bay through Davis Strait and enter the Labrador Sea where they continue south in the Labrador Current (Newell, 1993; Tang et al., 2004). Ice islands from northwest Greenland have been observed as far south as 42°N (Crawford, Crocker, et al., 2018). In this location offshore of Newfoundland, ice islands encounter warmer waters associated with the North Atlantic Current, which hastens their disintegration (Figure 2; Bigg et al., 1997).

3. Methods

3.1. The CI2D3 Database and Initial Data Subsetting

The geospatial CI2D3 Database contains >25,000 entries representing observations of >900 individual ice islands that were descendants of the large initial ice islands that calved from Petermann Glacier and other northwest Greenland ice tongues between 2008 and 2012 (Crawford, Crocker, et al., 2018; Desjardins et al., 2018). To generate the CI2D3 Database, ice islands were identified in SAR scenes obtained from the CIS archive. These were primarily RADARSAT-1 and -2 (Canadian Space Agency) ScanSAR Wide acquisitions with nominal resolutions of 100 m. A polygon was delineated to represent the surface extent of each identified ice island in ArcGIS (v. 10.2–10.5), and a number of geospatial and qualitative attribute fields were populated using customized geographic information system tools. Ice islands were tracked at a minimum 2-week observation interval. The lineage connection that is captured in the CI2D3 Database is illustrated in Figure 3a. These lineage connections are made between repeat observations of a tracked ice island, or between a "mother" ice island and the "daughters" that are created through their fracturing.

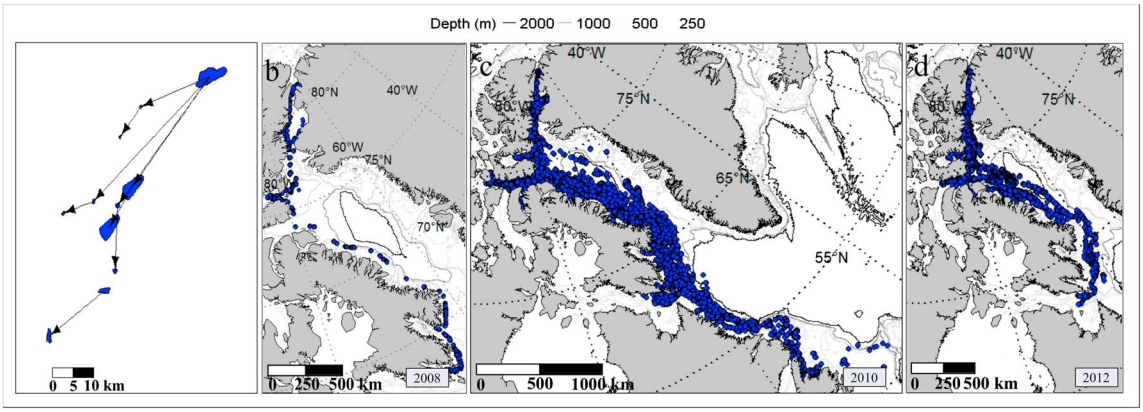

Figure 3. Illustration of Petermann ice island observations represented in the Canadian Ice Island Drift, Deterioration and Detection Database. (a) Example of the directional relationship (i.e., lineage connection) established between repeat observations of an ice island and between "daughter" ice islands resulting from the fracture of "mother" ice islands. All database entries associated with the (b) 2008, (c) 2010, and (d) 2012 Petermann Glacier calving events, represented as blue points. The database currently includes entries of ice islands that were observed up to 31 December 2013. When monitoring ended, ice islands totaling 2% and 70% of the original surface area associated with the 2010 and 2012 calving events remained in the study region.

Uncertainty in the digitized surface area, calculated as the coefficient of variation between database technicians, was 6.2% for monitored ice islands and 8.4% when an ice island was first identified in satellite imagery. (cf. Paul et al., 2013). Full details regarding the data sources, workflow, and uncertainty assessment associated with the CI2D3 Database are provided in Crawford, Crocker, et al. (2018). The database documentation (Crawford, Desjardins, et al., 2018) is found at https://wirl.carleton.ca/ci2d3. The database is housed at the Polar Data Catalogue, a public repository (https://www.polardata.ca/pdcsearch/PDCSearch.jsp?doi_id=12678).

This study focuses on the flux of ice islands following the largest three recent Petermann Glacier calving events. The database contains 332, 9,658, and 7,263 ice island observations associated with the 2008, 2010, and 2012 calving events, respectively (Figure 3). Ice islands associated with the 2008 calving event were monitored until there were no longer any identifiable ice islands >0.25 km^2 in the study area. Monitoring of the ice islands associated with the 2010 and 2012 calving events ended on 31 December 2013. The ice islands associated with the 2008, 2010, and 2012 calving events had been monitored for 1, 3.5, and 1.5 years after their respective calving events.

Finally, a note on terminology: The Manual of Ice defines an ice island fragment as a "piece of an ice island that has broken away from the main mass" (CIS, 2005). It is difficult to distinguish the "main mass" with increasing time after an initial glacier calving. For this reason, and also due to the overlap in sizes between ice islands and fragments from different sources and calving events, all individual pieces are referred to as "ice islands" in this study. The term *ice island* is not traditionally used to describe large tabular icebergs that originate from Antarctica. However, all Arctic and Antarctic large tabular icebergs are referred to as ice islands throughout this paper for simplicity. Smaller nontabular and tabular icebergs discussed in other publications are still referred to as "icebergs."

3.2. Size Distributions

We assessed the fit of several statistical distributions to the size-frequency distributions of PIIs originating from the 2010 and 2012 calving events. The size-frequency distribution of ice islands originating from the 2008 calving event was not used in this analysis due to the low number of individual ice islands associated with this calving event. Database entries were subset to include only the first representation of each ice island fragment per 2-week period to remove sampling bias. Eight of these periods, each separated by a period of approximately 6 months, served as "snapshots" to evaluate if the best fit distribution was consistent over time. The study area was divided into four spatial snapshots, regions of 10° latitude that broadly represent major water bodies (Table 1), to assess if the best fit distribution was consistent across the drift range of PIIs. Similar to the temporal assessment, only the first observation of an ice island

Table 1
Spatial Snapshots Used to Assess Variation in Size Distributions

Spatial snapshot	Water bodies	Latitude range (°N)
1	Nares Strait/northern Baffin Bay	≥75
2	Baffin Bay	<75 ≥65
3	Labrador Sea	<65 ≥55
4	southern Labrador Sea; North Atlantic	<55

that was observed multiple times as it drifted through a spatial region was included in each spatial snapshot. Only three ice islands associated with the 2012 Petermann Glacier calving event were associated with the third spatial snapshot. We omitted this snapshot from the distribution fitting analysis due to this small sample size.

Several probability distributions (power law, log-normal, normal, exponential, gamma, Weibull, and log-logistic) were fitted to the observed ice island size-frequency distributions at each temporal and spatial snapshot using R (v. 3.0.2; R Core Team, 2013). Truncation of the data set at 0.25 km^2 was accounted for using the fitdistrplus, FAdist, and poweRlaw R packages (Aucoin, 2015; Delignette-Muller et al., 2017; Gillespie, 2017). A comparison of the quality of the fitted distributions was conducted based on their individual Kolmogorov-Smirnov statistic using the truncgof R package (Wolter, 2015).

3.3. Meltwater Dispersal

The spatial dispersal of meltwater resulting from the drift and deterioration of the PIIs was calculated based on surface area and thickness change between each successive observation of the monitored ice islands in the CI2D3 Database. Surface area change was calculated from areal extent information captured in the database. Thickness change was estimated using basal and surface ablation modeling. Initial thicknesses of 76 ± 6 (1σ) and 182 ± 16 m were assigned to the ice islands created from the 2010 and 2012 calving events (Münchow et al., 2014). The thickness of the 2008 PII was estimated to be 62.3 ± 6.8 m based on the draft observed when it drifted over a mooring, deployed during the Canadian Arctic Through-flow project, at 80.5°N on 11 August 2008. Values of of 873 kg/m^3 (Crawford, Crocker, et al., 2018) and 1,025 kg/m^3 were assigned to ice density (ρ_i) and water density (ρ_w), respectively. Thickness was backcalculated for all of the ice islands associated with the 2008 calving event that were observed prior to this date (i.e., between 13 July and 11 August 2008) with the following basal and surface ablation models.

Basal ablation (M_b, m/s) was modeled by considering the turbulent exchange of heat across a flat plate (Weeks & Campbell, 1973). M_b is related to the differential velocity (Δu; m/s) between the ocean current and ice island drift and the difference in temperature (ΔT; ℃) between the underlying ocean water and the melting point (T_m) across its waterline L (m) with equation (1).

$$M_b = C \times \Delta u^{0.8} \frac{\Delta T}{L^{0.2}} \tag{1}$$

C was assigned a value of 1.3×10^{-5} $\cdot m^{-2/5} \cdot s^{-1/5} \cdot ℃^{-1}$. Crawford (2018), reports this value, after calibrating the forced-convection basal ablation model with field data collected from a PII. Following Kubat et al. (2007) and Løset (1993), T_m was calculated with equation (2), an empirical relationship that accounts for the influence of meltwater on the salinity of the ice-ocean boundary layer and, consequently, the melting point of the ice.

$$T_m = T_f \times e^{-0.19(T_e - T_f)} \tag{2}$$

In equation (2), T_e is the water temperature at the keel depth and T_f is the far-field freezing temperature of ocean water at the same depth (Broström et al., 2009; Løset, 1993). T_f is calculated with salinity (S; psu) and pressure (dbar) at the ice island keel depth (Fofonoff & Millard, 1983).

Equations (1) and (2) were forced with 5-day average ocean temperature and salinity data from a simulation with the 1/12° resolution (about 4 km in Baffin Bay) regional Arctic and Northern Hemisphere Atlantic configuration of the Nucleus for European Modelling of the Ocean (NEMO) v.3.4 ocean model (Madec and the NEMO team, 2015). This configuration covers the Arctic Ocean, as well as much of the Atlantic Ocean, with open boundaries at the Bering Strait and 20°S. The simulation is run from 2002 to 2016 using surface forcing from the Canadian Centre for Meteorological and Environmental Prediction's (Environment and Climate Change Canada) Global Deterministic Prediction System (GDPS) ReForcasts (CGRF) (Smith et al., 2014). Further details on the model setup, as well as evaluation in and around Baffin Bay, can be found in Hu et al. (2018) and Hughes et al. (2016).

The mean value associated with the drift of "PII-A" from the 2010 calving event (0.067 m/s), as modeled by the CIS, was assigned to Δu. The parameterization of Δu is a potential source of uncertainty for the M_b calculations within the thinning model (Bouhier et al., 2018; Jansen et al., 2007). A sensitivity analysis using the

2008 calving event was conducted to illustrate the effect of varying the assigned value of Δu; the assigned value of Δu was adjusted by 1σ (+0.047 m/s) to show the resulting variation in the magnitude of meltwater input dispersed through the study region following the 2008 Petermann Glacier calving event.

Surface ablation (M_s; m/day) was calculated with a temperature index melt model, where a degree-day factor (DDF; m water equivalent [w.e.]·°C^{-1}·day^{-1}) relates positive degree days (PDDs; °C· day) to an ablation magnitude (equation (3); Pellicciotti et al., 2005).

$$M_s = DDF \times PDD \tag{3}$$

A value of 6.4 mm w.e.·°C^{-1}·day^{-1} was assigned to the DDF parameter (Crawford et al., 2015). PDDs were calculated using hourly 2-m air temperature data from the CGRF data set (Smith et al., 2014). The ocean and atmospheric data for the NEMO or CGRF grid cell where the ice island was located at the time of observation were used, and the thinning of each ice island was then hindcast. The equations were run iteratively, so previous thinning was taken into account when determining the depth bin from which to extract T_e and S. Keel depth was also corrected for adjustments in hydrostatic equilibrium after each change in thickness.

The thinning experienced between successive ice island observations was calculated with M_b and M_s. The meltwater input was then calculated based on the volume lost due to thinning across the surface area of each ice island and the volume associated with decreases in surface area. Surface area loss was calculated between successive observations of a tracked ice island or determined from unaccounted surface area based on the combined surface extents of daughter ice islands following the fracturing of a mother ice island. Some ice islands associated with the 2010 calving event did not have a fully documented history. The thicknesses of these "orphan" ice islands were estimated based on the average melt rate of all other monitored ice islands. Two small (~1 km^2) orphan ice islands that were first observed ~2 years after the 2010 calving event were omitted from the analysis because we could not reasonably estimate their thickness.

The areal extent of individual ice islands occasionally fluctuated due to satellite imagery artifacts and digitization uncertainty. This occurred more frequently after a mother ice island fractured than between observations of an individual ice island that was monitored over time. Apparent increases in ice island volume were subtracted from previously calculated meltwater input to ensure that this extra volume was not double counted in the analysis, which would result in an overestimate of freshwater flux. Therefore, extent fluctuations do not alter net freshwater input associated with individual calving events so long as they are completely documented.

"Terminal" ice islands, referring to those that fell below the 0.25-km^2 monitoring threshold or otherwise became impossible to identify in SAR imagery, were converted to meltwater. Meltwater mass and volume were aggregated by 2-week time periods across a 50 × 50-km grid. The time-integrated meltwater flux was also calculated in milli-Sverdrups (mSv) across the same grid. To estimate meltwater discharge into the Baffin Island and Labrador currents, the meltwater flux was calculated after aggregating the meltwater input over larger regions of the study area.

4. Results

4.1. Overview of Ice Island Drift and Deterioration After Petermann Glacier Calving Events

The drift trajectories of ice islands associated with the 2008, 2010, and 2012 Petermann Glacier calving events generally followed a route south through Nares Strait and continued along the western edge of Baffin Bay and the Labrador Sea. The 2008 PII calved on 13 July with an initial surface area of 30.0 ± 2.5 km^2. Four other ice islands ranging from 0.3 ± 0.03 to 5.39 ± 0.5 km^2 that most likely calved directly from Petermann Glacier were also observed in the following days. The main ice island fractured twice in Nares Strait in August 2008 and was not observed to fracture again until May 2009, though its surface area did decrease from 21.8 ± 1.4 to 11.0 ± 0.7 km^2. This ice island rapidly deteriorated in the spring of 2009 when 15 small ice islands were generated. The last ice island linked to the 2008 calving event was observed at the mouth of Frobisher Bay, southeastern Baffin Island in July 2009 (Figure 4a).

At 292.7 ± 24.6 km^2, the 2010 PII was an order of magnitude larger than the 2008 PII, and a far greater number of ice islands were generated through its breakup (Figure 4b). Three smaller ice islands of 5.1 ± 0.4, 1.5 ± 0.1,

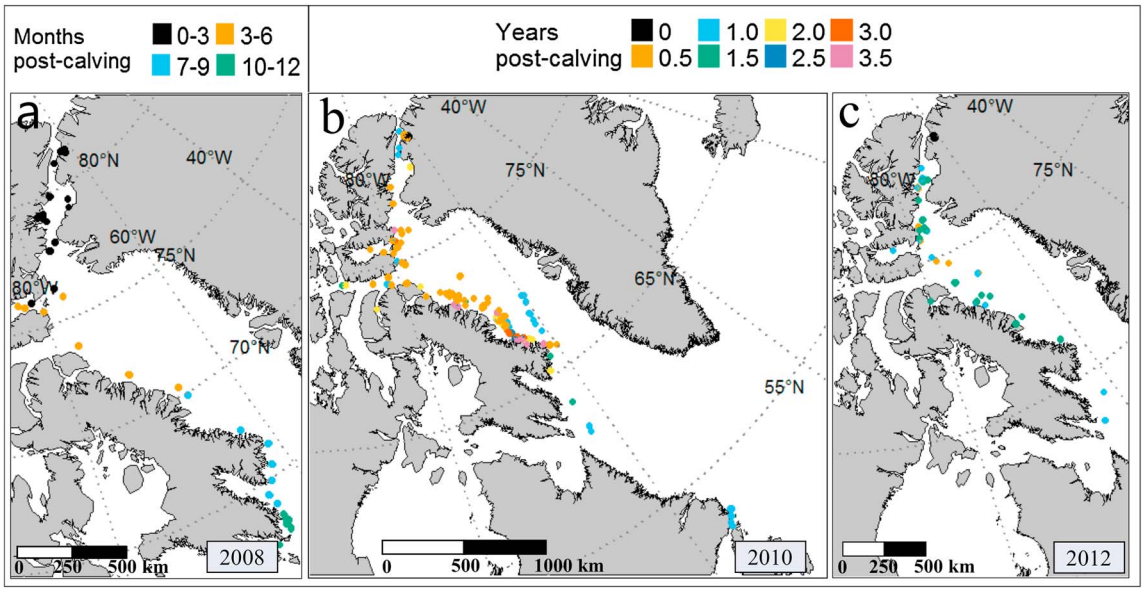

Figure 4. Ice island movement through the study area, color coded by time since calving, for the (a) 2008, (b) 2010, and (c) 2012 Petermann Glacier calving events. All observations associated with the 2008 calving over the relatively short monitoring period. Ice islands associated with the 2008 event were monitored until all ice islands were no longer identifiable (1 year post calving). The 2010 and 2012 events were subset to represent the "snapshots" of the ice island populations analyzed in the size distribution analysis. Ice islands associated with the 2010 and 2012 events were tracked for 3.5 and 1.5 years post calving, respectively. The coloring used for the temporal snapshots in Figures 4b and 4c correspond to the distributions shown in Figures 5 and 6, respectively.

and 2.6 ± 0.2 km^2 also calved on 5 August 2010, yielding a total loss of 20.0 ± 0.1 Gt of ice. The 2012 PII was initially 136.9 ± 11.5 km^2, or 21.8 ± 0.2 Gt. The CI2D3 Database follows the 2010 and 2012 PIIs until 31 December 2013. At this time, six ice islands associated with the 2010 calving event remained in the study area. The combined surface area of these ice islands represented 2% of the original surface extent of this calving event. Eighteen ice islands and 70% of the original surface extent of the 2012 calving event remained in the study area when monitoring ended.

4.2. Size Distributions

The ice island populations following the 2010 and 2012 Petermann Glacier calving events were consistently dominated by smaller ice island sizes. For example, the majority of ice islands were <1 km^2 for 80% of the assessed temporal and spatial snapshots (Figures 5 and 6). While smaller ice islands dominated the 2010 and 2012 size distributions, the same pattern was not seen for the 2008 data set. This was due to the limited fracturing experienced by the main ice island, which retained a relatively large surface area as it drifted through the study area.

Based on the Kolmogorov-Smirnov test statistic comparison, the observed size-frequency distributions of all spatial and temporal snapshots were best represented by a power law distribution (Figures 5 and 6). A log-logistic model provided the second best fit to the size-frequency distributions of over 90% of the tested snapshots. The power law, log-logistic, and Weibull distributions were all more representative of the observed size-frequency distributions than the log-normal distribution. This was the case for all tested temporal and spatial snapshots.

The slopes of the fitted power law models for each of the temporal and spatial snapshots (-2.1 to -1.5) are shown in the complementary cumulative distribution function plots of Figures 5 and 6. Here, P(surface area) refers to the proportion of observations of the ice island surface area less than or equal to the value given on the *x*-axis. The mean slope of the power law distributions fit to the 2010 snapshots was -1.7 (±0.2 standard deviation). The slopes associated with the power law fits to the 2012 snapshots had the same mean slope but a smaller standard deviation than the distributions fit to the 2010 snapshots (-1.7 ± 0.05), likely due to the shorter monitoring duration associated with the 2012 Petermann Glacier calving event.

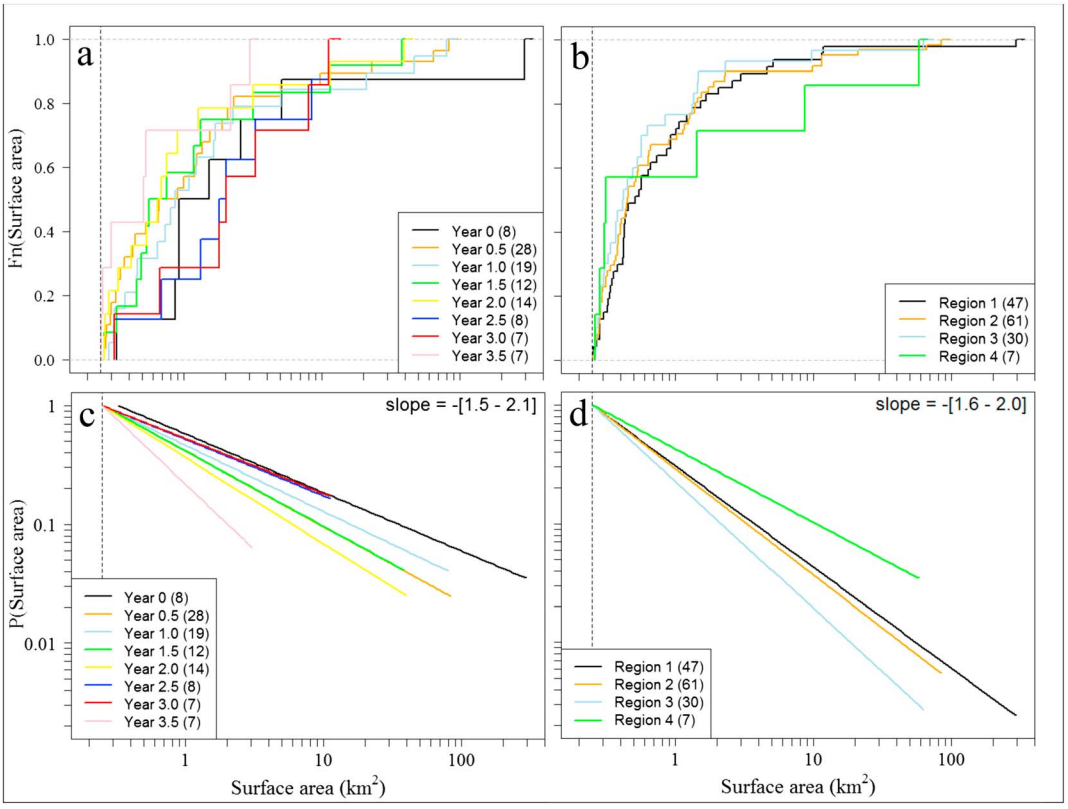

Figure 5. Ice island size distributions and distribution modeling (2010). Empirical cumulative size-frequency distributions of ice islands associated with the 2010 Petermann Glacier calving event by (a) temporal and (b) spatial snapshots. Power law model fits for the log-log complementary cumulative distribution function of ice island surface area for the same (c) temporal and (d) spatial snapshots. Values in parentheses refer to the number of ice island observations associated with the temporal or spatial snapshot. The vertical dotted line in each panel represents the 0.25-km^2 threshold under which ice islands were not regularly included in the Canadian Ice Island Drift, Deterioration and Detection Database and therefore were not considered in this analysis. The coloring of Figures 5a and 5c corresponds to that in Figure 4b.

4.3. Meltwater Dispersal

Approximately 2.1 Gt of freshwater was contained in the ice island that calved from Petermann Glacier in 2008. The ice island that calved in 2010 contained almost 10 times the amount of freshwater compared to the 2008 event. The initial ice island that calved in 2012 was less than half the extent of the 2010 ice island. However, the ice island that calved in 2012 had a mass of approximately 22 Gt, which was similar to the 2010 ice island due to a much greater thickness (Münchow et al., 2014). The magnitude of meltwater input into Nares Strait, Baffin Bay, and the Labrador Sea due to the deterioration of these three original ice islands is shown in Figure 7. We capture 100% and 65% of the freshwater associated with the original ice islands that calved from Petermann Glacier in 2008 and 2012, respectively (Figure 7). Due to uncertainty associated with the thickness of orphan ice islands and fluctuations in the digitized surface area of some monitored ice islands, the freshwater associated with the original 2010 calving event was overestimated by ~4% (Figure 7b).

A relatively large quantity of meltwater was input within and at the mouth of Petermann Fjord after each calving event. The meltwater flux in the Petermann Fjord reached 0.3 mSv in the first 2 weeks after the 2012 calving event, and 0.9 Gt of meltwater was input at this location over the time that the associated ice islands were monitored. The meltwater flux in the fjord was 7 times greater (2.0 mSv) after the 2010 Petermann Glacier calving event. In total, 2.8 Gt of meltwater input was calculated at this location following this calving event.

Ice island grounding in the northwest portion of Baffin Bay and along the continental shelf of Baffin Island resulted in relatively high meltwater inputs at these locations. One example was the approximately

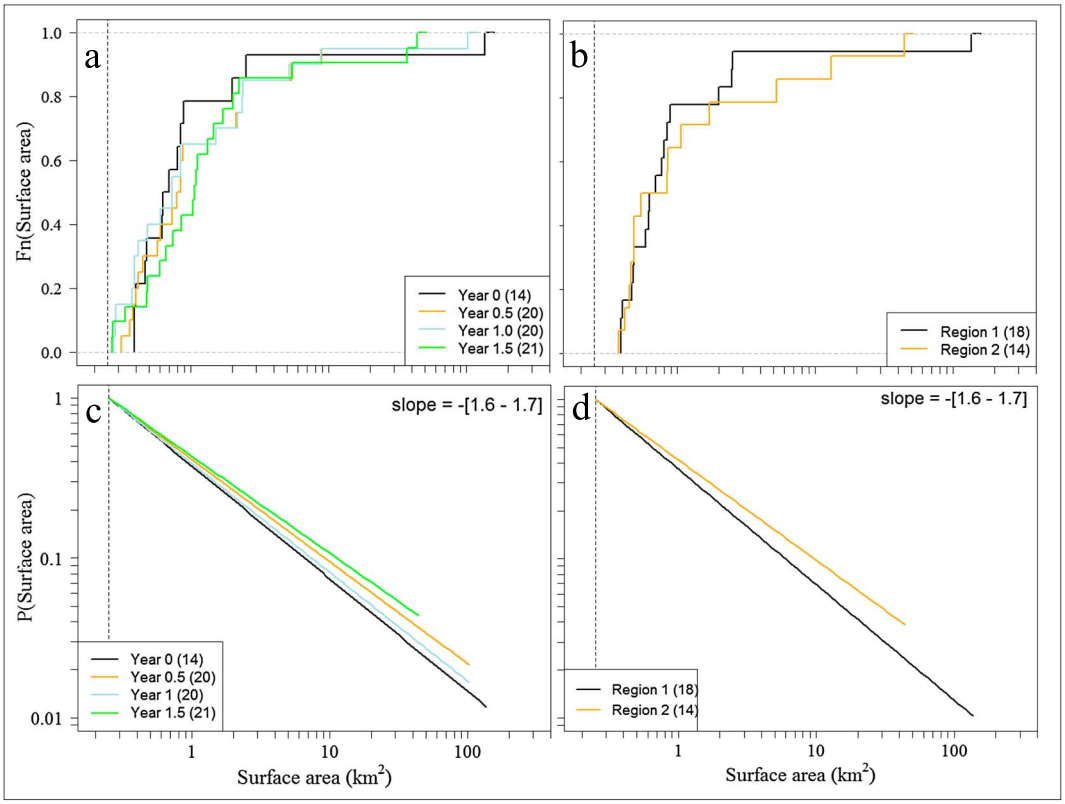

Figure 6. Ice island size distributions and distribution modeling (2012). Empirical cumulative size-frequency distributions of ice islands associated with the 2012 Petermann Glacier calving event by (a) temporal and (b) spatial snapshots. Power law model fits for the log-log complementary cumulative distribution function of ice island surface area for the same (c) temporal and (d) spatial snapshots. Values in parentheses refer to the number of ice island observations associated with the temporal or spatial snapshot. The vertical dotted line in each panel represents the 0.25-km^2 threshold under which ice islands were not regularly included in the Canadian Ice Island Drift, Deterioration and Detection Database and therefore were not considered in this analysis. The coloring of Figures 6a and 6c corresponds to that of Figure 4c.

0.4-mSv flux observed in the late summer of 2011 in the grid cell associated with "PII-B," an ice island that was grounded in this location for 15 months (Crawford et al., 2016). Increased meltwater input magnitudes and time-integrated fluxes also coincided with regions where ice islands fully deteriorated, or at least to the point that they were no longer tracked in the CI2D3 Database. For example, approximately 0.7 Gt, or 35% of the mass, of the 2008 ice island was input at the mouth of Frobisher Bay following a large breakup event (Figure 7a, lower right). Meltwater fluxes for individual grid cells in this region reached 0.1 mSv during this time. Large meltwater inputs were also observed off southern Labrador and Newfoundland where many ice islands that originated from the 2010 calving event fully deteriorated or fell below the CI2D3 Database monitoring threshold. The greatest meltwater flux into the Baffin Bay (0.7 mSv) and the Labrador Sea/North Atlantic region (0.9 mSv), which corresponds with the Baffin Island and Labrador currents, respectively, occurred approximately 1 year following the 2010 calving event.

The sensitivity analysis showed that the amount of meltwater input in a single 50 × 50-km grid cell varied by as much as 33% when the value assigned to Δu was varied by +1σ. However, the impact of varying Δu was more influential, relatively speaking, when minimal surface area reduction was taking place. This is a result of Δu being directly implicated in the calculation of basal ablation, which was the process causing the majority of deterioration during periods associated with smaller magnitudes of surface area reduction. The significant negative correlation between the relative difference in meltwater input and the surface area loss per grid cell ($r = -0.32$, $p \leq 0.05$) supports our conclusion that variation in Δu was most influential when little surface area reduction was taking place.

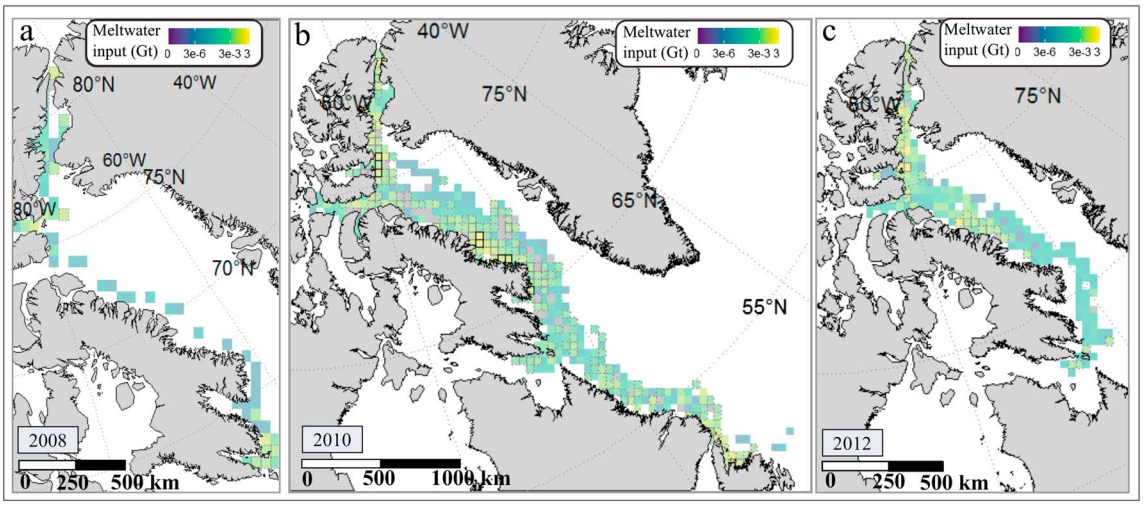

Figure 7. Spatial distribution of meltwater input, shown in gigatons (Gt), into the study area over the time period that the drift and deterioration of ice islands originating from the (a) 2008, (b) 2010, and (c) 2012 Petermann Glacier calving events were monitored. Ice islands associated with the 2008 event were monitored until all ice islands were no longer identifiable (1 year post calving). Ice islands associated with the 2010 and 2012 events were tracked for 3.5 and 1.5 years post calving, respectively. Locations where no ice islands were observed are denoted by the white background. Gray cells denote where freshwater flux could not be reasonably estimated due to fluctuation in ice island volume resulting from the digitization workflow and quality of the remotely sensed imagery used to generate the Canadian Ice Island Drift, Deterioration and Detection Database. The count of ice islands that were no longer monitored in the database ("terminal ice islands") is denoted by the cell outlines: gray dotted outline = 1 to 5; gray solid line = 6 to 10; black solid line = >10; no outline = no terminal ice islands. It is likely that freshwater input in these grid cells is overestimated since terminal ice islands were immediately converted to meltwater.

5. Discussion

5.1. Size Distributions

Approximately 80% of ice islands in the spatial and temporal snapshots were <10 km^2 (Figures 5 and 6). This supports previous findings that most mass will be contained within a few large ice islands, while the ice island population will be dominated by smaller ice islands, which are difficult to detect in SAR imagery (Rackow et al., 2017; Saper, 2011; Wesche & Dierking, 2015). Therefore, these smaller ice islands, icebergs, bergy bits, and growlers pose greater risks to offshore operations such as shipping and resource extraction (Saper, 2011). Iceberg charts are routinely produced in the North Atlantic where the resource extraction industry is active (Karlsen et al., 2001). However, the spatial coverage of these charts does not extend into the Canadian Arctic, and only ice islands >5 km in length are regularly included on regional sea ice charts (CIS, 2005).

The ice island generated after the 2008 calving event did not fracture over the majority of the time that it was monitored. For this reason, we did not include it in the size distribution analysis. Potential reasons why this ice island remained largely intact include its high relative thickness (i.e., the ratio of thickness to surface dimensions), high sea ice concentration, and/or a low number of internal weaknesses that can predispose an ice island to fracture by wave stress (Goodman et al., 1980; Orheim, 1980). Similar to our results for ice islands associated with the 2010 and 2012 calving events, Enderlin et al. (2016) found that a power law model reasonably represented iceberg size distributions in a Greenland fjord and used this to estimate growler populations. The finding that the size-frequency distributions of PIIs were best represented by a power law model can similarly inform future predictions of the size-frequency distributions of ice islands, which may be of particular interest to offshore industry concerned with these marine hazards. The mean slope of the power law distributions that were fit to the temporal and spatial snapshots in our study is very close to that reported for the size-frequency distribution of Antarctic ice islands (−1.5; Bouhier et al., 2018; Tournadre et al., 2016). This suggests that ice islands in both the Arctic and the Antarctic deteriorate through a complex set of fracture and fragmentation mechanisms and that these deterioration processes occur similarly across a range of ice island sizes (Kirkham et al., 2017; Tournadre et al., 2016).

In contrast, Kirkham et al. (2017) and Tournadre et al. (2012) found that the size-frequency distribution of smaller icebergs located further from glacier calving sites was better represented by a log-normal model.

Kirkham et al. (2017) explain that deterioration is increasingly dominated by a relatively small set of melt processes (e.g., forced convection and wave erosion) as icebergs travel away from source glaciers. Conversely, larger icebergs (and ice islands) are subject to a more complex set of deterioration processes (e.g., large-scale fracture, smaller-scale calving, and ablation). This results in a wide range of ice island surface areas and a situation in which a log-normal model can display characteristics that are similar to a power law model (Kirkham et al., 2017; Tournadre et al., 2016). Mathematically, log-normal models converge towards power law models as the variation in the variable of interest (i.e., surface area) increases. The quadratic term in the log-normal density function is then minimized and the linear term correspondingly becomes more influential (Mitzenmacher, 2004; Tournadre et al., 2016). The finding that the power law distribution provided the best fit for all temporal and spatial snapshots suggests that the complexity of deterioration processes to which the PIIs were subject did not substantially decrease over the study area or time period that they were monitored.

5.2. Meltwater Dispersal

While fracturing and fragmentation alter ice island size distributions, they also influence meltwater production. Fracturing causes further dispersal of meltwater as individual ice islands drift apart after a fracture event (Tournadre et al., 2012) and also increases the surface area to volume ratio, which will cause an ice island to be more susceptible to other meltwater-generating deterioration processes (e.g., wave erosion; Kirkham et al., 2017; Stern et al., 2017). The dispersal of meltwater with the drift and deterioration of icebergs and ice islands is often discussed in terms of the impact on fjord dynamics, local ocean properties, and ocean circulation patterns (Enderlin et al., 2016; Stern et al., 2015; Wagner & Eisenman, 2017).

The strength of the Atlantic Meridional Overturning Circulation (AMOC) is of concern when considering the increasing freshwater flux from the Greenland Ice Sheet and potential consequences to global ocean circulation and energy transfers (Bamber et al., 2012; Böning et al., 2016; Gillard et al., 2016; Yang et al., 2016). In their modeling studies, Gillard et al. (2016), Marson et al. (2018), and Wagner and Eisenman (2017) note that direct meltwater input from the Greenland Ice Sheet or via iceberg deterioration could affect deep-water convection in the North Atlantic and potentially lead to a slowdown of the AMOC. However, a sustained freshwater flux anomaly of at least 7 mSv in the North Atlantic is thought to be necessary to substantially slowdown the AMOC (Brunnabrend et al., 2015; Yang et al., 2016). For reference, the Baffin Island Current transports ~93 mSv of liquid freshwater to the northern Labrador Sea (Curry et al., 2014). Our study shows meltwater fluxes rose by 0.7 and 0.9 mSv in the Baffin Island and Labrador currents, respectively, after recent calving events at Petermann Glacier. Therefore, while this meltwater was likely transported to the North Atlantic, fluxes of this magnitude will not independently trigger a slowdown of the AMOC (Yang et al., 2016). However, such additions of meltwater do augment an already increasing meltwater flux from the Greenland Ice Sheet that concentrates in the Labrador Sea. This results in a freshening of the upper Labrador Sea, which could potentially weaken deep-water convection in this region (Yang et al., 2016). Further ocean modeling studies that focus on the fate of iceberg meltwater input at the ocean surface should be conducted to understand its role in regional ocean circulation patterns (Marson et al., 2018).

At a more local scale, large meltwater input was calculated within Petermann Fjord after the 2008, 2010, and 2012 calving events, and a maximum flux of 2.0 mSv was reached after the 2010 calving event. This input is a result of ice island melt as well as the reduction in ice island surface area while within the fjord due to fracture and other deterioration processes. This caused ice islands to fall under the 0.25-km^2 CI2D3 Database monitoring threshold, after which point their mass was included in the meltwater input calculation. The freshwater input in Petermann Fjord was likely overestimated as a result. We note that a layer between ~200- and 500-m depth in Petermann Fjord is highly influenced by a meltwater plume from basal ablation at the grounding line of the glacier (Johnson et al., 2011), and meltwater resulting from iceberg deterioration will likely remain above this layer. Meltwater input from ice island or iceberg deterioration could affect the physical composition of surface waters in Greenland fjords by influencing fjord circulation and altering the availability of heat for further glacier melt (Enderlin et al., 2016; Moon et al., 2018). Further research on the relationship between the sources of freshwater input in Petermann Fjord (i.e., glacial discharge, iceberg deterioration, and melt of the ice tongue) is necessary, and subsequent melt rates of the ice tongue and icebergs with the fjord would be an interesting addition to this research subject.

Outside Petermann Fjord, an elevated meltwater input was seen to coincide with grounding "hot spots" along the eastern coasts of Ellesmere, Devon, and Baffin islands. For example, the deterioration of the grounded "PII-B" at 69°N off the east coast of Baffin Island contributed to a meltwater flux of approximately 0.4 mSv in the corresponding grid cell. Stern et al. (2015) and Nacke (2016) are the few recent Arctic studies that focused on alterations to the physical and biological water column caused by ice island deterioration. The capacity for Arctic ice islands to impact the ocean ecosystem has previously been questioned due to the difference in ice island sizes and which nutrients limit productivity of the Arctic versus Antarctic ocean ecosystems. However, Smith et al. (2013) postulate that Arctic icebergs will impact the ocean column by promoting upwelling (as observed by Stern et al., 2015), decreasing stratification, increasing the delivery of nutrients, and increasing biological activity. Further in situ observations are necessary to support these hypotheses.

5.2.1. Meltwater Analysis Considerations

The distribution of meltwater by single Antarctic ice islands throughout their drift in the Southern Ocean has been documented by Helly et al. (2011), Jansen et al. (2007), and Schodlok et al. (2006). Likewise, regional meltwater input in the Antarctic has been estimated with models (Bigg et al., 2014; Gladstone et al., 2001; Martin & Adcroft, 2010; Merino et al., 2016; Stern et al., 2016) and analysis of the large Antarctic data sets compiled with altimeter, SAR, microwave radiometer, and optical data (Silva et al., 2006; Tournadre et al., 2012, 2015, 2016). However, it has not yet been possible to calculate more accurate ablation rates and determine the location and magnitude of meltwater inputs over the full size range of Antarctic ice islands due to lineage connections only being available for those $>$18.5 km in length (Merino et al., 2016). Lineage tracking within the CI2D3 Database removes this constraint and allows the spatial distribution of meltwater input to be determined.

Uncertainty in estimation of the magnitude and location of deterioration/meltwater input is introduced by the time interval between observations, the manual digitization workflow used in generating the CI2D3 Database, the assumed thickness of the initial ice islands, and modeled thinning rates. In regard to the latter, a constant value was assigned to Δu when modeling M_b. In reality Δu will fluctuate due to, for example, wind forces, the presence of sea ice, and ice island grounding. It is recommended that field campaigns be designed to collect in situ ice island drift and ocean current data to constrain the range of observed values of Δu and calibrate equation (1) for the drifting ice island case. Similar overestimation or underestimation of meltwater input within and outside of fjords will arise from assigning inappropriately high or low values to the C and DDF parameters when modeling M_b and M_s, respectively.

The conversion of ice islands that ceased to be monitored before they fully deteriorated introduces uncertainty to the estimated spatial distribution of meltwater, as does the occasional fluctuation of the areal surface extent of a monitored ice island. The meltwater associated with the small "terminal" ice islands represented approximately 30%, 40%, and 19% of the total meltwater input calculated after the 2008, 2010, and 2012 calving events, respectively. The locations of the final observations of these ice islands are denoted in Figure 7; however, it is likely that these ice islands later drifted out of these grid cells. Future studies could refine the meltwater input estimation by modeling the subsequent drift and deterioration of these small ice islands, but it is outside of the scope of this paper to do so. Increases in surface area-associated fluctuation in areal extents corresponded to 3%, 7%, and 8% of the original extents of the PIIs created in 2008, 2010, and 2012, respectively. Finally, it is possible that an ice island will travel through more than one NEMO or CGRF grid cell between observations. This is a potential limitation with respect to the environmental data assigned to hindcast the surface and basal ablation, especially when longer time intervals existed between observations of an individual ice island.

6. Conclusions

The CI2D3 Database was used to conduct the first deterioration analysis for the flux of ice islands generated after the 2008, 2010, and 2012 Petermann Glacier calving events. Hundreds of individual ice islands drifted through the eastern Canadian Arctic and sub-Arctic due to recurrent fracturing after initial calving events at Petermann Glacier. It was found that the size-frequency distributions of PIIs were well represented by a power law model. This was consistent across temporal and spatial snapshots, which suggests that fracturing caused by various mechanisms continued to be an important deterioration process as time elapsed from the

original calving event and as ice islands drifted through the study region. These results can inform shipping and natural resource extraction operations in the study area as to the likely distribution of ice hazard sizes after large Petermann Glacier calving events.

Ice island fracture does not directly produce meltwater. However, fracture does increase the surface area-to-volume ratio of the resulting ice islands, which will increase the susceptibility of resulting ice islands to other deterioration processes that do generate meltwater. We quantified the spatial distribution of meltwater input with the drift and deterioration of the 2008 (2.1 Gt), 2010 (20 Gt), and 2012 (22 Gt) PIIs. The calculated meltwater fluxes were not large enough to adversely affect the AMOC. However, this meltwater contributes to the increasing freshwater flux from the Canadian Arctic Archipelago and the Greenland Ice Sheet, which Yang et al. (2016) suggest could be weakening the stability of this important circulation system. Areas of augmented meltwater input after Petermann Glacier calving events included locations prone to grounding (i.e., the east coast of Baffin Island) and within Petermann Fjord. The impact of meltwater on ocean waters in relatively close proximity to ice islands has been more concertedly studied in the Antarctic than in the Arctic, and it is recommended that further research be dedicated to this topic in the Northern Hemisphere. For such studies, the size-distribution analysis presented in this study could be used for initializing general circulation models with iceberg components (Stern et al., 2016).

These investigations into the repercussions of Petermann Glacier calving events contribute to two dominant ice island research themes: ice islands as hazards and their role in meltwater dispersal from the major ice sheets. In total, the 2008, 2010, and 2012 PIIs were responsible for the greatest areal loss from any marine-terminating Greenland glacier monitored between 1999 and 2013 (Jensen et al., 2016). The 2010 calving event was almost double the annual ice discharge across the grounding line of Petermann Glacier (Rignot & Steffen, 2008) and reduced the area of the floating ice tongue by 25% (Nick et al., 2012). Increased ocean and atmospheric temperatures and reduced sea ice extents will continue to destabilize ice shelves (Liu et al., 2015; Shroyer et al., 2017), and a calving event >120 km^2 in surface extent is anticipated to occur at Petermann Glacier in the coming years (Münchow et al., 2016). The deterioration of the numerous ice islands generated after these large calving events will continue to be an important subject of study due to their hazard implications as well as their role in the distribution of freshwater from the major ice sheets.

Acknowledgments

We greatly appreciate all of the individuals who were involved in the creation of the CI2D3 Database. The CI2D3 Database is publically available under record number 12678 in the Polar Data Catalogue (https://www.polardata.ca/pdcsearch/PDCSearch.jsp?doi_id=12678) and is fully documented in Crawford, Desjardins, et al. (2018). The project received funding from Environment and Climate Change Canada and Polar Knowledge Canada, both within the Government of Canada, as well as funding for computing resources by the Canada Foundation for Innovation and the Ontario Research Fund. SAR scenes used to generate the CI2D3 Database were acquired from the Canadian Ice Service (Environment and Climate Change Canada) archive. We thank Doug King and Gregory Crocker (Geography and Environmental Studies, Carleton University), Shawn Kenny (Department of Civil and Environmental Engineering, Carleton University), and Douglas MacAyeal (Department of Geophysical Sciences, University of Chicago) for their reviews of the manuscript. Data from ice-profiling sonar in Kennedy Channel (e.g., ice island thickness) were collected with support from the Canadian Program for the International Polar Year within the Canadian Arctic Through-flow project (2006-SR1-CC-135). These data are available from archives maintained by Fisheries and Oceans Canada at the Institute of Ocean Sciences, Sidney, BC: Project name—Canadian Arctic Through-flow Study. Lead scientist—Dr. Humfrey Melling (humfrey.melling@dfo-mpo.gc.ca). Data from ice island modeling analyses are available from archives maintained by Environment and Climate Change Canada at the Canadian Ice Service, Ottawa, ON. Lead scientist—Hai Tran (hai.tran@canada.ca). The numerical modeling using NEMO was funded by Natural Sciences and Engineering Research Council (NSERC) of Canada to Paul G. Myers, including a Discovery Grant (rgpin 227438-09) and Climate Change and Atmospheric Research Grants (VITALS—RGPCC 5 433898 and the Canadian Arctic Geotraces program—RGPCC 433848). The experiment was run on Jasper, a Compute Canada computational cluster, and the model output is held at a repository at the University of Alberta, Edmonton, AB. Lead scientist—Paul Myers (pmyers@ualberta.ca). Visit http://knossos.eas.ualberta.ca/anha/anhatable.html to access the model output. We also thank G. Smith for the CGRF forcing fields that were made available by Environment and Climate Change Canada. Personal academic funding was provided to A. Crawford through the W. Garfield Weston Foundation and NSERC.

References

Aucoin, F. (2015). Package 'FAdist'. CRAN Repository. v. 2.2. Retrieved from https://github.com/tpetzoldt/FAdist

Bamber, J., van den Broeke, M., Ettema, J., Lenaerts, J., & Rignot, E. (2012). Recent large increases in freshwater fluxes from Greenland into the North Atlantic. *Geophysical Research Letters*, *39*, L19501. https://doi.org/10.1029/2012GL052552

Bigg, G. R., Marsh, R., Wilton, D., & Ivchenko, V. (2014). B31—A giant iceberg in the Southern Ocean. *Ocean Challenge*, *20*, 32–34.

Bigg, G. R., Wadley, M. R., Stevens, D. P., & Johnson, J. A. (1997). Modelling the dynamics and thermodynamics of icebergs. *Cold Regions Science and Technology*, *26*(2), 113–135. https://doi.org/10.1016/S0165-232X(97)00012-8

Böning, C. W., Behrens, E., Biastoch, A., Getzla, K., & Bamber, J. L. (2016). Emerging impact of Greenland meltwater on deepwater formation in the North Atlantic Ocean. *Nature Geoscience*, *9*(7), 523–527. https://doi.org/10.1038/NGEO2740

Bouhier, N., Tournadre, J., Rémy, F., & Gourves-Cousin, R. (2018). Melting and fragmentation laws from the evolution of two large southern ocean icebergs. *The Cryosphere*, *12*(7), 2267–2285. https://doi.org/10.5194/tc-12-2267-2018

Broström, G., Melsom, A., Sayed, M., & Kubat, I. (2009). Iceberg modeling at met.no: Validation of iceberg model. Report 17/2009 (36 pp.). Norwegian Meteorological Institute, Blindern, Norway.

Brunnabend, S.-E., Schröter, J., Rietbroek, R., & Kusche, J. (2015). Regional sea level change in response to ice mass loss in Greenland, the West Antarctic and Alaska. *Journal of Geophysical Research: Oceans*, *120*, 7316–7328. https://doi.org/10.1002/2015JC011244

Budd, W. F., Jacka, T. H., & Morgan, V. I. (1980). Antarctic iceberg melt rates derived from size distributions and movement rates. *Annals of Glaciology*, *1*, 103–112. https://doi.org/10.3189/S0260305500017079

Canadian Ice Service. (2005). Manual of standard procedures for observing and reporting ice conditions (146 pp.). Environment Canada, Ottawa, Canada: Canadian Ice Service.

Crawford, A., Desjardins, L., Saper, R., & Mueller, D. (2017). Canadian Ice Island Drift, Deterioration and Detection (CI2D3) Database documentation V1.0. Project documentation (20 pp.). Water and Ice Research Lab, Department of Geography and Environmental Studies Carleton University, Ottawa, Canada.

Crawford, A., Desjardins, L., Saper, R., Mueller, D., & Stewart-Jones, E. (2018). Canadian Ice Island Drift, Deterioration and Detection (CI2D3) Database Documentation [V1.1] (18 pp.). Ottawa, Canada: Water and Ice Research Laboratory, Carleton University.

Crawford, A., Mueller, D. R., Humphreys, E., Carrieres, T., & Tran, H. (2015). Surface ablation model evaluation on a drifting ice island in the Canadian Arctic. *Cold Regions Science and Technology*, *110*, 170–182. https://doi.org/10.1016/j.coldregions.2014.11.011

Crawford, A. J. (2018). Ice island deterioration (Doctoral dissertation). Retrieved from CURVE. Ottawa, Canada: Department of Geography and Environmental Studies, Carleton University. https://curve.carleton.ca/ea21063d-8cca-42c7-a7e7-56a89322cb88

Crawford, A. J., Crocker, G., Mueller, D., Desjardins, L., Saper, R., & Carrieres, T. (2018). The Canadian Ice Island Drift Deterioration and Detection (CI2D3) Database. *Journal of Glaciology*, *64*(245), 517–521. https://doi.org/10.1017/jog.2018.36

Crawford, A., Wadhams, P., Wagner, T., Stern, A., Abrahamsen, P., Church, I., et al. (2016). Journey of an Arctic ice island. *Oceanography*, *29*(2). https://doi.org/10.5670/oceanog.2016.30

Curry, B., Lee, C. M., Petrie, B., Moritz, R. E., & Kwok, R. (2014). Multiyear volume, liquid freshwater and sea ice transports through Davis Strait, 2004–10. *Journal of Physical Oceanography*, *44*(4), 1244–1266. https://doi.org/10.1175/JPO-D-13-0177.1

Delignette-Muller, M.-L., Dutang, C., Pouillot, R., Denis, J.-B., & Siberchicot, A. (2017). Package 'fitdistrplus'. CRAN Repository. v.1.0–-1.99. Retrieved from https://lbbe.univ-lyon1.fr/fitdistrplus.html

Desjardins, L., Crawford, A., Mueller, D., Saper, R., Schaad, C., Stewart-Jones, E., & Shepherd, J. (2018). Canadian Ice Island Drift, Deterioration and Detection Database (CI2D3 Database) [v1.1]. Canadian Cryospheric Information Network (CCIN), Waterloo, Canada. https://doi.org/10.21963/12678

Duprat, L. P., Bigg, G. R., & Wilton, D. J. (2016). Enhanced Southern Ocean marine productivity due to fertilization by giant icebergs. *Nature Geoscience*, *9*(3), 219–221. https://doi.org/10.1038/NGEO2633

Enderlin, E. M., Carrigan, C. J., Kochtitzky, W. H., Cuadros, A., Moon, T., & Hamilton, G. S. (2018). Greenland iceberg melt variability from high-resolution satellite observations. *The Cryosphere*, *12*, 1–17. https://doi.org/10.5194/tc-2017-185

Enderlin, E. M., Hamilton, G. S., Straneo, F., & Sutherland, D. A. (2016). Iceberg meltwater fluxes dominate the freshwater budget in Greenland's iceberg-congested glacial fjords. *Geophysical Research Letters*, *43*, 11,287–11,294. https://doi.org/10.1002/2016GL070718

Fissel, D. B. (1982). Tidal currents and inertial oscillations in northwestern Baffin Bay. *Arctic*, *35*(1), 201–210.

Fletcher, T., Budge, J., Robinson, E., Prigmore, E., Hill, J., Madsen, N., et al. (2016). The Antarctic Iceberg Tracking Database. Retrieved from http://www.scp.byu.edu/data/iceberg/database1.html

Fofonoff, N.P., & Millard, R.C. (1983). Algorithms for computation of fundamental properties of seawater. *Technical Papers in Marine Science* (Vol. 44). UNESCO, Paris, France.

Fuglem, M., & Jordaan, I. (2017). Risk analysis and hazards of ice islands. In L. Copland & D. Mueller (Eds.), *Arctic ice shelves and ice islands* (pp. 395–415). Dordrecht, Netherlands: Springer. https://doi.org/10.1007/978-94-024-1101-0_15

Gillard, L. C., Hu, X., Myers, P. G., & Bamber, J. L. (2016). Meltwater pathways from marine terminating glaciers of the Greenland Ice Sheet. *Geophysical Research Letters*, *43*, 10,873–10,882. https://doi.org/10.1002/2016GL070969

Gillespie, C. (2017). Package "poweRlaw"—Analysis of heavy tailed distributions. CRAN Repository. v. 0.70.1. Retrieved from https://github.com/csgillespie/poweRlaw

Gladstone, R. M., Bigg, G. R., & Nicholls, K. W. (2001). Iceberg trajectory modeling and meltwater injection in the Southern Ocean. *Journal of Geophysical Research*, *106*, 19,903–19,915. https://doi.org/10.1029/2000JC000347

Goodman, D. J., Wadhams, P., & Squire, V. A. (1980). The flexural response of a tabular ice island to ocean swell. *Annals of Glaciology*, *1*(1), 23–27. https://doi.org/10.3189/S0260305500016906

Haas, C. (2012). Distribution and thickness of different sea ice types and extreme ice features in the Beaufort Sea. *Field Report for the Beaufort Regional Environmental Assessment*.

Hamley, T. C., & Budd, W. F. (1986). Antarctic iceberg distribution and dissolution. *Journal of Glaciology*, *32*(111), 242–251. https://doi.org/10.1017/S0022143000015574

Helly, J. J., Kaufmann, R. S., Stephenson, G. R., & Vernet, M. (2011). Cooling, dilution and mixing of ocean water by free-drifting icebergs in the Weddell Sea. *Deep Sea Research Part II: Topical Studies in Oceanography*, *58*(11-12), 1346–1363. https://doi.org/10.1016/j.dsr2.2010.11.010

Higgins, A. K. (1989). North Greenland ice islands. *Polar Record*, *25*(154), 207–212. https://doi.org/10.1017/S0032247400010809

Higgins, A. K. (1991). North Greenland glacier velocities and calf ice production. *Polarforschung*, *60*(1), 1–23.

Hu, X., Sun, J., Chan, T. O., & Myers, P. G. (2018). Thermodynamic and dynamic ice thickness contributions in the Canadian Arctic Archipelago in NEMO-LIM2 numerical simulations. *The Cryosphere*, *12*(4), 1233–1247. https://doi.org/10.5194/tc-12-1233-2018

Hughes, K. G., Klymak, J. M., Hu, X., & Myers, P. G. (2016). Water mass modification and mixing rates in a 1/12° simulation of the Canadian Arctic Archipelago. *Journal of Geophysical Research: Oceans*, *122*, 803–820. https://doi.org/10.1002/2016JC012235

Jacka, T. H., & Giles, A. B. (2007). Antarctic iceberg distribution and dissolution from ship-based observations. *Journal of Glaciology*, *53*(182), 341–356. https://doi.org/10.3189/002214307783258521

Jansen, D., Schodlok, M., & Rack, W. (2007). Basal melting of A-38B: A physical model constrained by satellite observations. *Remote Sensing of Environment*, *111*(2-3), 195–203. https://doi.org/10.1016/j.rse.2007.03.022

Jensen, T. S., Box, J. E., & Hvidberg, C. S. (2016). A sensitivity study of annual area change for Greenland ice sheet marine terminating outlet glaciers: 1999–2013. *Journal of Glaciology*, *62*(231), 72–81. https://doi.org/10.1017/jog.2016.12

Johnson, H. L., Münchow, A., Falkner, K. K., & Melling, H. (2011). Ocean circulation and properties in Petermann Fjord, Greenland. *Journal of Geophysical Research*, *116*, C01003. https://doi.org/10.1029/2010JC006519

Karlsen, H. G., Bille-Hansen, J., Hansen, K. Q., Andersen, H. S., & Skourup, H. (2001). Distribution and variability of icebergs in the eastern Davis Strait 63°N to 68°N. Report No. 2001–1 (38 pp.). Bureau of Minerals and Petroleum, Greenland Survey, ASIAQ, Denmark.

Kirkham, J. D., Rosser, N. J., Wainwright, J., Vann Jones, E. C., Dunning, S. A., Lane, V. S., et al. (2017). Drift-dependent changes in iceberg size-frequency distributions. *Scientific Reports*, *7*(1), 15991. https://doi.org/10.1038/s41598-017-14863-2

Kubat, I., Sayed, M., Savage, S. B., Carrieres, T., & Crocker, G. (2007). An operational iceberg deterioration model. *Proceedings of the 17th International Offshore and Polar Engineering Conference* (pp. 652–657). International Society of Offshore and Polar Engineers. Lisbon, Portugal.

Liu, Y., Moore, J. C., Cheng, X., Gladstone, R. M., Bassis, J. N., Liu, H., et al. (2015). Ocean-driven thinning enhances iceberg calving and retreat of Antarctic ice shelves. *Proceedings of the National Academy of Sciences*, *112*(11), 3263–3268. https://doi.org/10.1073/pnas.1415137112

Long, D. G., Ballantyne, J., & Bertoia, C. (2002). Is the number of Antarctic icebergs really increasing? *Eos*, *83*(42), 473–474.

Løset, S. (1993). Numerical modelling of the temperature distribution in tabular icebergs. *Cold Regions Science and Technology*, *21*(2), 103–115. https://doi.org/10.1016/0165-232X(93)90001-O

Luckman, A., Padman, L., & Jansen, D. (2010). Persistent iceberg groundings in the western Weddell Sea, Antarctica. *Remote Sensing of Environment*, *114*(2), 385–391. https://doi.org/10.1016/j.rse.2009.09.009

Madec G & the NEMO team (2015). NEMO ocean engine. No. 27. Note du Pole de modélisation de l'Institut Pierre-Simon Laplace, France. 396 pp.

Marson, J., Myers, P., Hu, X., & Le Sommer, J. (2018). Using vertically-integrated ocean fields to characterize Greenland icebergs' distribution and lifetime. *Geophysical Research Letters*, *45*, 4208–4217. https://doi.org/10.1029/2018GL077676

Martin, T., & Adcroft, A. (2010). Parameterizing the fresh-water flux from land ice to ocean with interactive icebergs in a coupled climate model. *Ocean Modelling*, *34*(3–4), 111–124. https://doi.org/10.1016/j.ocemod.2010.05.001

McGonigal, D., Hagen, D., & Guzman, L. (2011). Extreme ice features distribution in the Canadian Arctic. In *Proceedings of the 21st International Conference on Port and Ocean Engineering under Arctic Conditions*. POAC11–045. Montreal, Canada.

Merino, N., Le Sommer, J., Durand, G., Jourdain, N. C., Madec, G., Mathiot, P., & Tournadre, J. (2016). Antarctic iceberg melt over the Southern Ocean: Climatology and impact on sea ice. *Ocean Modelling*, *104*, 99–110. https://doi.org/10.1016/j.ocemod.2016.05.001

Mitzenmacher, M. (2004). A brief history of generative models for power law and lognormal distributions. *Internet Mathematics*, *1*(2), 226–251. https://doi.org/10.1080/15427951.2004.10129088

Moon, T., Sutherland, D. A., Carroll, D., Felikson, D., Kehrl, L., & Straneo, F. (2018). Subsurface iceberg melt key to Greenland fjord freshwater budget. *Nature Geoscience*, *11*(1), 49–54. https://doi.org/10.1038/s41561-017-0018-z

Mueller, D.R., Crawford, A., Copland, L., & Van Wychen, W. (2013). Ice island and iceberg fluxes from Canadian High Arctic sources. *Report to the Northern Transportation Assessment Initiative* (23 pp.). Innovation Policy Branch, Transport Canada, Ottawa, Canada.

Münchow, A., Padman, L., & Fricker, H. A. (2014). Interannual changes of the floating ice shelf of Petermann Gletscher, North Greenland, from 2000 to 2012. *Journal of Glaciology*, *60*(221), 489–499. https://doi.org/10.3189/2014JoG13J135

Münchow, A., Padman, L., Washam, P., & Nicholls, K. (2016). The ice shelf of Petermann Gletscher, North Greenland, and its connection to the Arctic and Atlantic oceans. *Oceanography*, *29*(4), 84–95. https://doi.org/10.5670/oceanog.2016.101

Nacke, M. (2016). Characterization of the coastal marine environment in the vicinity of a grounded iceberg, Canadian Arctic Archipelago (Master's thesis). Retrieved from CURVE. Ottawa, Canada: Department of Geography and Environmental Studies, Carleton University. https://curve.carleton.ca/d8f40d5e-a4c8-455e-a810-cf0b19daf157

National Aeronautics and Space Administration (2010). Ice island calves off the Petermann Glacier. Retrieved from http://earthobservatory.nasa.gov/IOTD/view.php?id=45112 Accessed 13 May 2015.

National Aeronautics and Space Administration (2012). GMS: Petermann Ice Island 2012. Retrieved from http://svs.gsfc.nasa.gov/cgi-bin/details.cgi?aid=11114 Accessed 23 June 2016.

National Aeronautics and Space Administration (2017). Massive iceberg breaks off from Antarctica. Retrieved from https://www.nasa.gov/feature/goddard/2017/massive-iceberg-breaks-off-from-antarctica Accessed 17 January 2018.

National Geophysical Data Center (2006). ETOPO2v2 2-minute Global Relief Model. National Geophysical Data Center: Boulder, United States.

Newell, J. P. (1993). Exceptionally large icebergs and ice islands in eastern Canadian waters: A review of sightings from 1900 to present. *Arctic*, *46*(3), 205–211.

Nick, F. M., Luckman, A., Vieli, A., van der Veen, C. J., van As, D., van de Wal, R. S. W., et al. (2012). The response of Petermann Glacier, Greenland, to large calving events, and its future stability in the context of atmospheric and oceanic warming. *Journal of Glaciology*, *58*(208), 229–239. https://doi.org/10.3189/2012JoG11J242

Orheim, O. (1980). Physical characteristics and life expectancy of tabular Antarctic icebergs. *Annals of Glaciology*, *1*, 11–18. https://doi.org/10.3189/S0260305500016888

Paul, F., Barrand, N. E., Baumann, S., Berthier, E., Bolch, T., Casey, K., et al. (2013). On the accuracy of glacier outlines derived from remote-sensing data. *Annals of Glaciology*, *54*(63), 171–182. https://doi.org/10.3189/2013AoG63A296

Pellicciotti, F., Brock, B., Strasser, U., Burlando, P., Funk, M., & Corripio, J. (2005). An enhanced temperature-index glacier melt model including the shortwave radiation balance: Development and testing for Haut Glacier d'Arolla, Switzerland. *Journal of Glaciology*, *51*(175), 573–587. https://doi.org/10.3189/172756505781829124

Peterson, I. K. (2011). Ice island occurrence on the Canadian East Coast. In *Proceedings of the 21st International Conference on Port and Ocean Engineering under Arctic Conditions*. POAC11–044. Montreal, Canada.

Peterson, I. K., Prinsenberg, S. J., Pittman, M., & Desjardins, L. (2009). The drift of an exceptionally-large ice island from the Petermann Glacier in 2008. In *Proceedings of the 20th International Conference on Port and Ocean Engineering under Arctic Conditions* (pp. 130–140). Luleå, Sweden.

R Core Team (2013). R: A language and environment for statistical computing. R Foundation for Statistical Computing: Vienna, Austria.

Rackow, T., Wesche, C., Timmermann, R., Hellmer, H. H., Juricke, S., & Jung, T. (2017). A simulation of small to giant Antarctic iceberg evolution: Differential impact on climatology estimates. *Journal of Geophysical Research: Oceans*, *122*, 3170–3190. https://doi.org/10.1002/2016JC012513

Raiswell, R., Hawkings, J. R., Benning, L. G., Baker, A. R., Death, R., Albani, S., et al. (2016). Potentially bioavailable iron delivery by iceberg-hosted sediments and atmospheric dust to the polar oceans. *Biogeosciences*, *13*(13), 3887–3900. https://doi.org/10.5194/bg-13-3887-2016

Rignot, E., & Steffen, K. (2008). Channelized bottom melting and stability of floating ice shelves. *Geophysical Research Letters*, *35*, L02503. https://doi.org/10.1029/2007GL031765

Romanov, Y. A., Romanova, N. A., & Romanov, P. (2012). Shape and size of Antarctic icebergs derived from ship observation data. *Antarctic Science*, *24*(01), 77–87. https://doi.org/10.1017/S0954102011000538

Sackinger, W. M., Shoemaker, H. D., Serson, H., Jeffries, M. O., & Yan, M.-H. (1985). Ice islands as hazards to Arctic offshore production structures, in *Proceedings of the 17th Annual Offshore Technology Conference* (14 pp.). OTC 4943. Houston, United States.

Saper, R. (2011). Preliminary research plan for glacial ice hazards (40 pp.). Report prepared for the Canadian Ice Service, Environment Canada, Ottawa, Canada.

Schodlok, M. P., Hellmer, H. H., Rohardt, G., & Fahrbach, E. (2006). Weddell Sea iceberg drift: Five years of observations. *Journal of Geophysical Research*, *111*, C06018. https://doi.org/10.1029/2004JC002661

Shroyer, E. L., Padman, L., Samelson, R. M., Münchow, A., & Stearns, L. A. (2017). Seasonal control of Petermann Gletscher ice-shelf melt by the ocean's response to sea-ice cover in Nares Strait. *Journal of Glaciology*, *63*(238), 324–330. https://doi.org/10.1017/jog.2016.140

Silva, T. A. M., Bigg, G. R., & Nicholls, K. W. (2006). Contribution of giant icebergs to the Southern Ocean freshwater flux. *Journal of Geophysical Research*, *111*, C03004. https://doi.org/10.1029/2004JC002843

Smith, G. C., Roy, F., Mann, P., Dupont, F., Brasnett, B., Lemieux, J.-F., et al. (2014). A new atmospheric dataset for forcing ice-ocean models: Evaluation of reforecasts using the Canadian Global Deterministic Prediction System: CGRF dataset for forcing ice-ocean models. *Quarterly Journal of the Royal Meteorological Society*, *140*(680), 881–894. https://doi.org/10.1002/qj.2194

Smith, K. L. (2011). Free-drifting icebergs in the Southern Ocean: An overview. *Deep Sea Research Part II: Topical Studies in Oceanography*, *58*(11–12), 1277–1284. https://doi.org/10.1016/j.dsr2.2010.11.003

Smith, K. L., Sherman, A. D., Shaw, T. J., & Sprintall, J. (2013). Icebergs as unique Lagrangian ecosystems in polar seas. *Annual Review of Marine Science*, *5*(1), 269–287. https://doi.org/10.1146/annurev-marine-121211-172317

Stern, A. A., Adcroft, A., & Sergienko, O. (2016). The effects of Antarctic iceberg calving-size distribution in a global climate model. *Journal of Geophysical Research: Oceans*, *121*, 5773–5788. https://doi.org/10.1002/2016JC011835

Stern, A. A., Adcroft, A., Sergienko, O., & Marques, G. (2017). Modeling tabular icebergs submerged in the ocean. *Journal of Advances in Modeling Earth Systems*, *9*, 1948–1972. https://doi.org/10.1002/2017MS001002

Stern, A. A., Johnson, E., Holland, D. M., Wagner, T. J. W., Wadhams, P., Bates, R., et al. (2015). Wind-driven upwelling around grounded tabular icebergs. *Journal of Geophysical Research: Oceans*, *120*, 5820–5835. https://doi.org/10.1002/2015JC010805

Stuart, K. M., & Long, D. G. (2011). Tracking large tabular icebergs using the SeaWinds Ku-band microwave scatterometer. *Deep Sea Research Part II: Topical Studies in Oceanography*, *58*(11–12), 1285–1300. https://doi.org/10.1016/j.dsr2.2010.11.004

Tang, C. C., Ross, C. K., Yao, T., Petrie, B., DeTracey, B. M., & Dunlap, E. (2004). The circulation, water masses and sea-ice of Baffin Bay. *Progress in Oceanography*, *63*(4), 183–228. https://doi.org/10.1016/j.pocean.2004.09.005

Tournadre, J., Bouhier, N., Girard-Ardhuin, F., & Rémy, F. (2015). Large icebergs characteristics from altimeter waveforms analysis. *Journal of Geophysical Research: Oceans*, *120*, 1954–1974. https://doi.org/10.1002/2014JC010502

Tournadre, J., Bouhier, N., Girard-Ardhuin, F., & Rémy, F. (2016). Antarctic icebergs distributions 1992–2014. *Journal of Geophysical Research: Oceans*, *121*, 327–349. https://doi.org/10.1002/2015JC011178

Tournadre, J., Girard-Ardhuin, F., & Legrésy, B. (2012). Antarctic icebergs distributions, 2002–2010. *Journal of Geophysical Research*, *117*, C05004. https://doi.org/10.1029/2011JC007441

Wagner, T. J. W., & Eisenman, I. (2017). How climate model biases skew the distribution of iceberg meltwater: Biases in iceberg meltwater distribution. *Geophysical Research Letters*, *44*, 3691–3699. https://doi.org/10.1002/2016GL071645

Weeks, W. F., & Campbell, W. J. (1973). Icebergs as a fresh-water source: An appraisal. *Journal of Glaciology*, *12*(65), 207–233. https://doi.org/10.1017/S0022143000032044

Wesche, C., & Dierking, W. (2015). Near-coastal circum-Antarctic iceberg size distributions determined from synthetic aperture radar images. *Remote Sensing of Environment*, *156*, 561–569. https://doi.org/10.1016/j.rse.2014.10.025

Wolter, T. (2015). Package 'truncgof'. CRAN Repository. v. 0.6–0. Retrieved from https://CRAN.R-project.org/package=truncgof

Yang, Q., Dixon, T. H., Myers, P. G., Bonin, J., Chambers, D., van den Broeke, M. R., et al. (2016). Recent increases in Arctic freshwater flux affects Labrador Sea convection and Atlantic overturning circulation. *Nature Communications*, *7*, 10525. https://doi.org/10.1038/ncomms10525